Interactive Visual Analysis of Perfusion Data

Steffen Oeltze, *Student Member, IEEE*, Helmut Doleisch, *Member, IEEE*, Helwig Hauser, *Member, IEEE*, Philipp Muigg, and Bernhard Preim

Abstract—Perfusion data are dynamic medical image data which characterize the regional blood flow in human tissue. These data bear a great potential in medical diagnosis, since diseases can be better distinguished and detected at an earlier stage compared to static image data. The wide-spread use of perfusion data is hampered by the lack of efficient evaluation methods. For each voxel, a time-intensity curve characterizes the enhancement of a contrast agent. Parameters derived from these curves characterize the perfusion and have to be integrated for diagnosis. The diagnostic evaluation of this multi-field data is challenging and time-consuming due to its complexity. For the visual analysis of such datasets, feature-based approaches allow to reduce the amount of data and direct the user to suspicious areas.

We present an interactive visual analysis approach for the evaluation of perfusion data. For this purpose, we integrate statistical methods and interactive feature specification. Correlation analysis and Principal Component Analysis (PCA) are applied for dimension reduction and to achieve a better understanding of the inter-parameter relations. Multiple, linked views facilitate the definition of features by brushing multiple dimensions. The specification result is linked to all views establishing a focus+context style of visualization in 3D. We discuss our approach with respect to clinical datasets from the three major application areas: ischemic stroke diagnosis, breast tumor diagnosis, as well as the diagnosis of the coronary heart disease (CHD). It turns out that the significance of perfusion parameters strongly depends on the individual patient, scanning parameters, and data pre-processing.

Index Terms—Multi-field Visualization, Visual Data Mining, Time-varying Volume Data, Integrating InfoVis/SciVis

---

1 INTRODUCTION

Compared to static image data, where the morphology of anatomic and pathological structures is represented with high spatial resolution, dynamic image data characterize functional processes, such as metabolism and blood flow, which is often essential to detect diseases at an early stage or to discriminate pathologies with very similar morphology. Important examples of these data are functional MRI, where activations of brain areas are measured, dynamic SPECT, where metabolic processes are imaged, and perfusion imaging, where the blood flow is represented. We focus on perfusion data which are acquired to support essential diagnostic tasks, e.g., cerebral perfusion for stroke diagnosis, the assessment of tumors, and perfusion of the myocardium (heart muscle) for CHD diagnosis.

In perfusion imaging, the distribution of contrast agents (CA) is registered to assess blood flow and tissue kinetics. For each voxel, a time-intensity curve (*TIC*) characterizes the CA enhancement. How long it takes until the maximum amount of CA is delivered, which maximum is achieved, as well as other parameters are derived from these curves for medical diagnosis. The derived parameters represent a special instance of multi-field data which is becoming more and more important in medicine [3], [11]. They are substitutes for physiological parameters such as tumor perfusion and vessel permeability [5]. The integrated analysis of several parameters in a suspicious region is essential. For the diagnosis of ischemic stroke, e.g., if the blood flow is delayed in a particular region, it is crucial to evaluate if the overall blood flow is also reduced [17].

To streamline the integrated analysis of perfusion parameters, we present a visual analysis approach incorporating pre-processing and statistical methods as well as feature specification steps. Motion cor-

rection and noise reduction are fundamental pre-processing issues to achieve a reliable correspondence of voxels over time. Since the different parameters are derived from the same TIC, it is likely that some parameters correlate with each other. We apply a correlation analysis and a PCA [15] to achieve a better understanding of the inter-parameter relations and to simplify and to speed-up the diagnosis by reducing the complexity of the multi-field data. Besides its complexity, the non-standardized parameter domain, which depends on the scanning protocol, complicates the diagnostic evaluation. For the visual analysis of such data, feature-based approaches allow to direct the user to suspicious regions and to reduce the amount of data. Our approach integrates methods for an interactive feature specification of high-dimensional complex features in multi-field data. Multiple, linked views facilitate the definition of features which can be complex and/or hierarchically described by brushing multiple dimensions. Non-binary brushes account for the uncertainty involved in the inspection of a non-standardized parameter domain. Furthermore, they represent a natural mapping of irreversibly damaged or malignant tissue, suspicious or reversibly damaged tissue and healthy tissue to focus, near-focus and context. The specification result from all views is linked to a 3D view, establishing a focus+context style of visualization. The 3D representation of the perfusion parameters within their anatomic context allows a localization of the specification result.

Our visual analysis approach primarily addresses medical researchers seeking for a better understanding of which perfusion parameters are crucial for specific diagnostic tasks and how imaging parameters influence the expressiveness of perfusion parameters. This research is motivated by contradictory recommendations in medical research papers, e.g., [1] and [25] for CHD diagnosis.

This paper is structured as follows: In Sec. 2, we give an overview on the medical background in perfusion diagnosis and on correlation analysis and PCA. Prior and related work on the application of Info-Vis techniques for the analysis of multi-field data as well as on the visual analysis of perfusion data are presented in Sec. 3. In Sec. 4, we describe our analysis approach. The application of the approach to clinical perfusion datasets from ischemic stroke diagnosis, breast tumor diagnosis, and CHD diagnosis, is discussed in Sec. 5. The last section will summarize and conclude the paper.

- *Steffen Oeltze and Bernhard Preim are with the Department of Simulation and Graphics, University of Magdeburg, Magdeburg, Germany, E-mail: {stoeltze|preim}@isg.cs.uni-magdeburg.de.*
- *Helmut Doleisch and Philipp Muigg are with the VRVis Research Center, Vienna, Austria, E-mail: {Doleisch|Muigg}@VRVis.at.*
- *Helwig Hauser is with the Department of Informatics, University of Bergen, Bergen, Norway, E-mail: Helwig.Hauser@uib.no.*

2 MEDICAL AND TECHNICAL BACKGROUND

This section gives a brief overview on perfusion diagnosis and acquaints the reader with the basics of correlation analysis and PCA.

2.1 Perfusion Diagnosis

In perfusion imaging, a CA is injected intravenously and its distribution is measured by a repeated acquisition of subsequent images covering the volume of interest. The CA provides signal changes in the acquired 4D data (3D+time). In case of a perfusion defect, the corresponding region exhibits an abnormal change in signal intensities. The spatial resolution and quality of perfusion data are worse than those of static data. High temporal resolution can only be achieved at the expense of lower spatial resolution and image quality.

Particularly CT, PET, SPECT and MRI data are employed for perfusion imaging. In the following, we only consider MR perfusion, since MRI is the most widespread perfusion imaging technique for breast tumor diagnosis. It outperforms CT in stroke diagnosis, since the entire brain can be scanned (instead of a single slice with CT) and it has shown to have at least a similar sensitivity and specificity in comparison to PET and SPECT in CHD diagnosis.

Perfusion Parameters. For the diagnosis, regions of interest in healthy and suspicious tissue are defined, and TICs—averaged over all voxels in the selected region—are analyzed. Depending on the application area, different sets of parameters, derived from the curves, are relevant. However, some parameters are of general interest (see Fig. 1). Before we describe these parameters, we introduce three parameters necessary for a reliable evaluation.

The *CA arrival* represents the point in time when the signal enhancement actually starts, whereas $Time_{End}$ refers to the end of the first CA passage. The *Baseline* represents the average intensity before *CA arrival* (see Fig. 1). These parameters are determined to focus the evaluation of the TIC to the relevant portion. Assessing perfusion considering the actual *CA arrival*, $Time_{End}$ and the *Baseline* is essential to compare analysis results from different scanning devices and patients. Major diagnostically relevant parameters are:

- *Peak Enhancement (PE)*. The maximum value (between *CA arrival* and $Time_{End}$) normalized by subtracting the *Baseline*. The *PE* separates the time interval between *CA arrival* and $Time_{End}$ into a phase of CA *wash-in* followed by the CA *wash-out*.

- *Time To Peak (TTP)*. The time until *PE* occurs, normalized by subtracting *CA arrival* time. This parameter allows to assess if the blood supply is delayed in a particular region.

- *Integral*. For the time interval between *CA arrival* and $Time_{End}$, the area between the curve and the *Baseline*—the approximated integral—is computed. Together, *PE* and *Integral* may give a hint on reduced blood flow.

- *Mean Transit Time (MTT)*. In the time interval used for the integral calculation, MTT specifies the first momentum of the curve. It is normalized by subtracting *CA arrival* time.

- The *Slope* characterizes the steepness of the curve during wash-in. Depending on the temporal resolution, different regression methods are used to characterize the curve progression. The term *Up-Slope* in cardiac diagnosis relates to the maximum slope between two or three subsequent time-steps during wash-in. In tumor perfusion studies, the related parameter *MiTR* (Maximum intensity to Time Ratio) is determined; it is computed as PE/TTP and it is thus an average slope.

- The *DownSlope* characterizes the steepness of the descending curve during wash-out and is computed similar to the *Slope*, however, with a negative sign.

The parameters are derived per voxel and stored in separate *parameter volumes* (3D). As a major pre-processing step, noise reduction is often solved by conventional filters, such as Gaussian. Lysaker et al. [19] introduced a filter for 4D data that better preserves features based on the simulation of a diffusion process. Motion-correction is the second major pre-processing task, carried out to establish a valid inter-pixel correspondence. It is essential when breathing, heartbeat, patient movement, or muscle relaxation occur. The motion correction algorithm developed by Rueckert et al. is widely used [26].
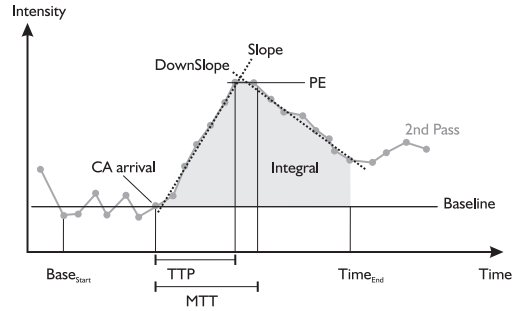

Fig. 1. A typical time-intensity curve in myocardial perfusion with a significant first pass and an alleviated second pass of contrast agent traversal annotated with the essential parameters to evaluate the first pass. Similar curves are observed in cerebral perfusion.

2.2 Correlation and Principal Component Analysis

Correlation analysis reveals whether variables vary independently of each other or are (inversely) proportional. The amount of correlation is represented by the so-called *correlation coefficient (r)*. In the following, we assume a matrix $A^{m \times n}$ representing n variables (perfusion parameters) and m observations (voxels of the *parameter volumes*). The symmetric matrix $R^{n \times n}$ of correlation coefficients is then computed based on the covariance matrix C of A. A value of $r_{ij} = -1$ indicates a perfect inversely proportional relationship, whereas a value of $r_{ij} = 1$ corresponds to a perfect proportional relationship. A value of $r_{ij} = 0$ relates to non-correlated variables. Besides R, an equally-sized symmetric matrix P of p-values is computed for testing the hypothesis of no correlation. If a particular p-value is < 0.05, the correlation is considered significant. Müller et al. [21] suggest that the user may exclude variables from a PCA that strongly correlate with each other. Otherwise, these variables might misleadingly strengthen certain trends.

The PCA is a technique from multivariate statistics to detect variables from multi-dimensional data that may be redundant. For dimension reduction, these variables may be grouped together. Furthermore, PCA explains the structure of relationships between variables and thus provides additional insight into the data. The PCA results in new variables, the so-called *principal components*. Each principal component (*pc*) represents a single axis in a new orthogonal coordinate space (*pc-space*)—generated by a variance maximum rotation of the original data space. The first pc (*pc*1) explains most of the variance in the original data, the second pc (*pc*2) most of the remaining variance, etc.

Before applying a PCA, it is often reasonable to standardize the data. This is necessary, if the variables have not been measured in the same units or if their variance is substantial. For standardization, A is centered around its mean and then each column of A is divided by its standard deviation. This step is often referred to as *Auto-scaling*. One way to compute the pc's is to apply a *Singular Value Decomposition (SVD)*. As a result, the SVD returns matrices $PCS^{n \times n}$, $scores^{m \times n}$ and a vector containing the eigenvalues $\lambda^{1 \times n}$ of C. Each column of PCS consists of n *loadings* representing the weights for the linear combination of the n original variables. The *scores* are the coordinates of the original data transformed into *pc-space*. The vector λ represents the variances explained by the n pc's.

According to Müller et al. [21], the PCA results may be exploited in several ways, e.g., to detect prominent trends in the data. These trends are represented by the pc's. The *loadings* indicate how individual variables correlate with these trends. The eigenvalues of C may be applied to neglect less significant trends (low values correspond to a low variance explained by the corresponding pc). A major problem involved in interpreting PCA results is the difficulty to relate trends to the original variables [21]. Therefore, Müller et al. [21] suggest to oppose the *scores* and the original variables in a scatterplot. Another approach they recommend is to present the *scores* in their spatial frame of reference (the original perfusion data). Furthermore, linking & brushing should be applied to relate the *scores* to the original variables.

3 PRIOR AND RELATED WORK

This section describes prior and related work on the application of InfoVis techniques for the analysis of multi-field data as well as on the visual analysis of perfusion data.

Visual Exploration of Multi-field Data. Our visualization concepts extend ideas from general systems for analyzing and exploring multidimensional image data such as [11]. Due to the absence of standardized intensity values and the high variability of image scanners and patient data, the analysis of perfusion is a typical exploratory analysis task where visual data mining techniques are essential.

Closely related concepts were presented by Gresh and Rogowitz in the WEAVE system [11]. In particular, we employ their concept of tightly integrating a 3D visualization with multiple statistical representations, connected by brushing facilities applied to scatterplot representations. Similar to their exploratory scenarios, we also attempt to quickly compare and correlate variables. Inspired by their approach, Doleisch et al. developed the SimVis framework for interactive feature specification for CFD data in previous work [8], [9]. In [3], the concepts of Gresh and Rogowitz have been optimized for the interactive work with very large medical multi-field datasets and extended by the integration of analysis techniques from pattern classification.

Visual Exploration of Perfusion Data. Basic visualization techniques for exploring perfusion data were described by [2] (focus on tumor perfusion) and [17] (focus on cerebral perfusion). The cinematic depiction of gray scale images in a movie loop gives an impression of the enhancement pattern [5]. *Subtraction images* depict the intensity difference between two selected points in time, thus, emphasizing regions where the CA is absorbed. However, they do not provide quantitative temporal and spatial information, which could make the diagnostic results more reproducible. Color-coded parameter maps [17] reveal the regional distribution of selected perfusion parameters. However, the analysis of parameter combinations in a tiled visualization requires a mental integration of suspicious regions.

Multiparameter visualizations, integrating several perfusion parameters in one image, were introduced in [16] and [23]. Different kinds of multivariate color scales, color icons and colored height fields were discussed. Flexible lenses were used to integrate the visualization of a foreground parameter (in the lens region) with a background parameter. In particular for Dynamic Contrast-Enhanced MRI Mammography (DCE-MRIM) data with its high spatial resolution, direct volume rendering techniques have been explored. A color-coded Closest Vessel Projection was presented in [16]. Coto et al. [6] employ two-level volume rendering and importance driven volume rendering to focus volume rendered images to previously segmented breast lesions. This work is the closest to our work since also linking & brushing was employed to select regions of interest. However, they did not consider the perfusion parameters described in Sec. 2.1. Instead, they only considered the intensity values and the enhancement in a subtraction image. The *application profile flags* presented by [20] may be used to immediately integrate TICs into a visualization, thus supporting the mental integration of the curve parameters and the display of the original perfusion data. Finally, [14] describe highly interactive 3D visualizations of DCE-MRIM data in a virtual reality environment.

Analysis of Perfusion Data. Another venue of analyzing perfusion data relates to a statistical analysis as well as mining and knowledge discovery techniques. In particular, the classification of DCE-MRIM data by means of artificial neural networks and clustering techniques is an active research area [4, 22, 28]. As an example, Twellmann et al. [28] applied an artificial neural network architecture which combines unsupervised and supervised techniques for voxel-by-voxel classification of temporal kinetic signals derived from DCE-MRIM data. Chen et al. [4] developed a fuzzy c-means clustering-based technique to automatically identify characteristic kinetic curves from segmented breast lesions in DCE-MRIM data. Nattkemper and Wissmueller [22] described the application of self-organized maps to time curve features of DCE-MRIM data and discussed how the results may be visually represented as color-coded cross-sections. The automatic classification may be useful in a screening setting in order to replace the opinion of a second radiologist or to direct a radiologist to suspicious regions.

4 A PERFUSION DATA ANALYSIS APPROACH

This section describes our visual analysis approach independent of a specific application area. However, the included figures have been generated based on cerebral perfusion data to illustrate the approach by means of a real-world example (see also Sec. 5.1).

The approach consists of three major components (see Fig. 2): a pre-processing component, a component for statistical analysis, and a component for interactive feature specification in multi-field data. For the work presented here, these components have each been implemented in Me*VisLab*[1], a platform for medical image processing and visualization, *MATLAB*[2], and the framework *SimVis*[3].
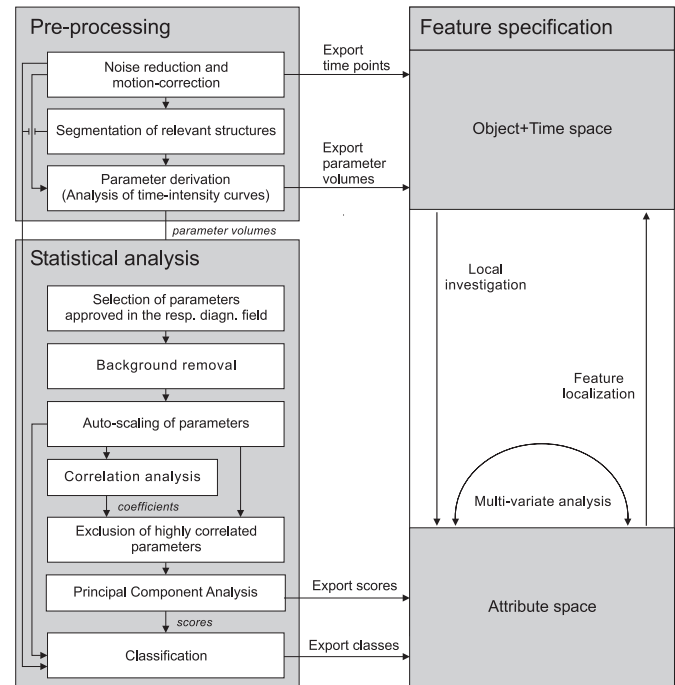

Fig. 2. Schematic representation of our perfusion data analysis approach consisting of a pre-processing component, a component for statistical analysis, and a component for interactive feature specification.

4.1 Pre-processing

The original 4D perfusion data serves as input for the pre-processing component. Here, the data is noise reduced applying a Gaussian kernel and motion-corrected according to [26]. The separate time points (3D data) are exported and may, e.g., serve as context information during the visual analysis. For some applications, such as ischemic stroke or CHD diagnosis, it is useful to restrict the computation of perfusion parameters to relevant structures (brain tissue or ventricles of the heart). A variety of segmentation algorithms has been integrated into Me*VisLab*. The perfusion parameters are derived voxel-wise for the segmented regions and exported separately as *parameter volumes*. These volumes serve as input for the feature specification as well as for the statistical component. The segmentation part may be skipped, if the entire dataset must be analyzed.

4.2 Statistical Analysis

At the beginning of the statistical analysis, the user is presented a list containing the perfusion parameters which have been approved in his or her diagnostic field of interest (see Sec. 5.1-5.3). The user may refine this initial set resulting in a new set $\{P_k\}$ of k parameters. In a

---

[1]Product of MeVis Research; www.mevislab.de

[2]Product of the MathWorks, Inc.; www.mathworks.com

[3]Developed by the VRVis Research Center, Vienna; www.simvis.at

next step, the background voxels within the *parameter volumes* corresponding to $\{P_k\}$ are identified to restrict further computations to the anatomic structures. Based on the histogram of one of these *parameter volumes*, the background voxels are identified (the highest peak in the histogram) and excluded from further analysis (*Background removal*). The decision may be refined by defining a threshold. The indices of the remaining m voxels VOX_{relev} are stored in a vector ID_{relev}. Then, the perfusion parameter matrix $A^{m \times k}$ is constructed considering only the voxels referred to by ID_{relev}. As discussed in Sec. 2.2, the PCA may require a standardization of its input to deliver meaningful results. Since the perfusion parameters have not been measured in the same units, *Auto-scaling* is applied to A resulting in $A_{std}^{m \times k}$.

To evaluate the relationships between several parameters, a correlation analysis is carried out resulting in matrices R and P. In order to consider only significant correlations, P is examined for values < 0.05. The correlation coefficients in R corresponding to the remaining values are set to 0 (no correlation). A visual representation of R now enables the user to identify parameters that are highly correlated (see Fig. 3). A scatterplot matrix is generated by plotting all columns in A_{std} against each other. The background color of each plot has been chosen according to the respective value in R. A color scale has been designed that visually separates negative and positive coefficients. Furthermore, it emphasizes strong correlations (coefficients < -0.9 or > 0.9). The diagonal of the scatterplot matrix shows a histogram for each parameter. All axes limits are set based on the respective inner quartile range such that outlier values are not displayed. The visualization of R in Fig. 3 shows the following strong correlations: *Integral* $\leftrightarrow PE$, *PE* $\leftrightarrow$ *MiTR*, *PE* $\leftrightarrow$ *Slope*, *Slope* $\leftrightarrow$ *MiTR* and *Slope* $\leftrightarrow$ *DownSlope* (inversely proportional). Since parameters *PE* and *Slope* strongly correlate with three other parameters respectively, they may be excluded from further processing. This results in the Matrix $A_{corr}^{m \times l}$, where l is the number of remaining parameters.
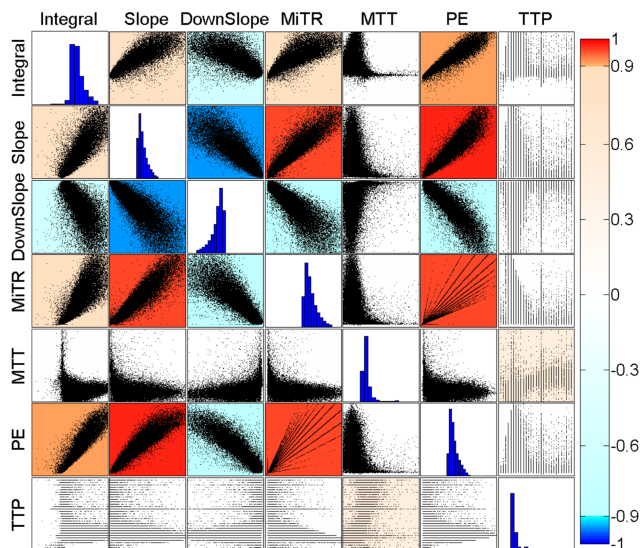

Fig. 3. Scatterplot matrix of perfusion parameters. The background color of each plot is chosen according to the respective correlation coefficient. The color scale is designed such that strong correlations (< -0.9 or > 0.9) are emphasized. The diagonal of the matrix shows a histogram for each parameter. All axes limits are set based on the respective inner quartile range such that outlier values are not displayed.

In a next step, a PCA is carried out based on A_{corr} resulting in the matrices $PCS^{l \times l}$, $scores^{m \times l}$ and a vector $\lambda^{1 \times l}$ (recall Sec. 2.2). To detect trends in the data, the *loadings* in PCS are visualized in a bar chart (see Fig. 4, crosshatched bars). However, the PCA does not only reveal the trends but it orders them by their significance—expressed by the variances in λ. To incorporate this significance in the visualization, the *loadings* in column $i, i \in [1, l]$ of PCS are weighted with
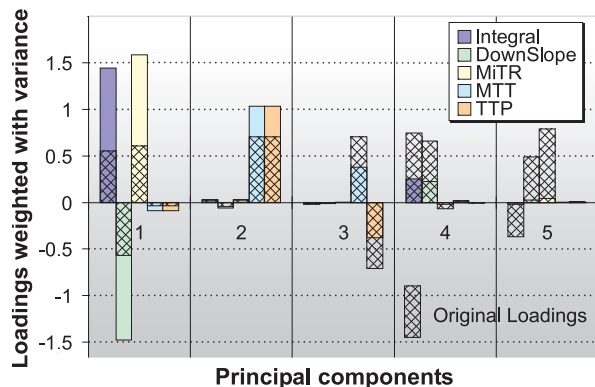

Fig. 4. Principal components and their *loadings* for the parameters. The original loadings are visualized as crosshatched bars. To incorporate the significance of each trend, these *loadings* are weighted with the variance explained by the corresponding pc (filled bars).

$\lambda(1, i)$ according to [21] (see Fig. 4, filled bars). The plot in Fig. 4 reveals a major trend represented by $pc1$. This trend is determined by the parameters *Integral*, *DownSlope* and *MiTR*. The positive *loadings* of *Integral* and *MiTR* indicate a direct proportional relationship, whereas the negative *loading* of *DownSlope* indicates an inversely proportional relationship. To relate the trends to the original perfusion parameters, their *scores* are exported for a later processing within the feature specification component.

The end of the statistical analysis constitutes a classification step which has not yet been implemented. However, related work indicates that in particular techniques to classify DCE-MRIM data are promising to detect suspicious regions (see Sec. 3).

4.3 Feature Specification

The interactive feature specification of data coming from the pre-processing as well as from the statistical analysis stage of our approach is carried out in a framework employing the SimVis technology [8], [9]. SimVis was previously developed for the analysis of 3D time-dependent flow simulation data, but has recently been extended to cope also with multiple other data types, e.g., 3D weather radar data and 3D medical data. A data converter has been implemented to transform medical RAW data into the SimVis data-format.

In SimVis, multiple linked views are used to concurrently show, explore, and analyze different aspects of multi-field data. 3D views of the volume (also over time) can be used next to several types of attribute views, e.g., scatterplots or histograms. Interactive feature specification is usually performed in these attribute views. The user chooses to visually represent selected data attributes in such a view, thereby gaining insight into the selected relations within the data. Then, the interesting subsets of the data are interactively brushed directly on the screen (see Fig. 5(b) for an example). The result of such a brushing operation is reintegrated into the data in form of a synthetic data attribute $DOI_j \in [0, 1]$ (*degree of interest (DOI) attribution* of the data, compare to Furnas [10]). This DOI attribution is used in the 3D views of the analysis setup to visually discriminate the interactively specified features from the rest of the data in a focus+context visualization style which is consistent in all (linked) views [13].

In the SimVis system *smooth brushing* [9] (enabling fractional DOI values) as well as the logical combination of brushes for the specification of *complex features* [8] are supported. A smooth brush results in a trapezoidal DOI function around the main region of interest in the attribute views. To enable the integration of a flexible derived data concept, a data calculator module with a respective graphical user interface has been added. New attributes can be derived from existing ones and thereafter are available for investigation in all linked views.

There are several different purposes of the interactive feature specification process and the resulting exploration and analysis steps, of which the most important are:
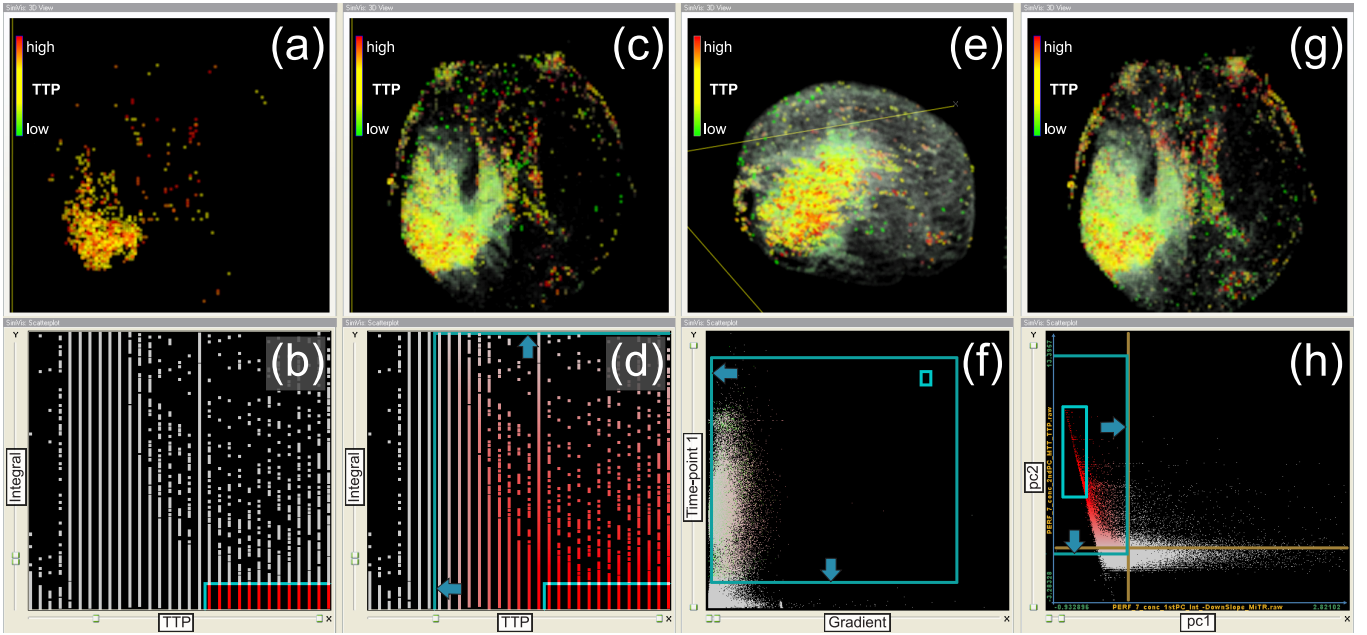
Fig. 5. Ischemic stroke diagnosis. High *TTP* and low *Integral* values (delayed and diminished perfusion) have been brushed in a scatterplot *(b)*. As a result, the infarction core is revealed in *(a)* applying *TTP* for color-coding. In *(d)*, a near-focus region (arrows point at its borders) is defined by means of smooth brushing. The updated visualization in *(c)* gives a hint on the location of "tissue at risk" (greenish area). In *(e)*, the brain is rotated to gain a better impression of the over-all extension of the infarction in 3D. Furthermore, the shape of the brain is indicated by a smooth brushing applied on the gradient magnitude computed from a single time point of the perfusion data *(f)*. Interestingly, a smooth brushing of the *scores* of *pc*1 and *pc*2 *(h)* yields a very similar result *(g)* compared to *(c)*. The brown lines in *(h)* represent the zero-axes.

- *Feature localization*: to search for places in the 3D domain of the data where certain feature characteristics are present. In the SimVis approach, the user can brush features in attribute views and concurrently localize the respective feature in the 4D (3D+time) volume domain.

- *Multi-variate analysis*: to investigate multi-variate data properties by specifying a feature in one attribute view and at the same time analyzing the DOI distribution with respect to other data attributes in other attribute views (through view linking).

- *Local investigation*: to inspect the values of selected data attributes with respect to certain spatiotemporal subsets of the 3D volume domain. In the SimVis system, the user can also load spatial as well as temporal data references into attribute views—brushing these kinds of data attributes then yields features which are specified according to their spatiotemporal extents.

5 APPLICATION

Our perfusion data analysis approach has been applied to 5 datasets so far (1 from ischemic stroke diagnosis, 2 from breast tumor diagnosis and 2 from CHD diagnosis). These datasets are representative for the respective diagnostic field concerning spatial and temporal resolution. Due to space restrictions, not all analysis results can be discussed here. Therefore, the reader is referred to our supplementary website: *wwwisg.cs.uni-magdeburg.de/cv/VAoPD/*. It contains additional analysis results, high-resolution versions of all images included in this paper and a video to illustrate the interactive aspect of the analysis.

Pre-processing. All datasets have been noise-reduced applying a Gaussian kernel. The datasets from breast tumor and CHD diagnosis have been motion-corrected according to [26]. In the dataset from ischemic stroke diagnosis, the brain tissue has been segmented by means of a watershed-algorithm [12]. In the datasets from CHD diagnosis, the myocardium has been semi-automatically segmented in each slice applying a live-wire technique [27]. The resulting contours have been propagated over all time points. The parameter derivation has been restricted to the segmentation results.

5.1 Ischemic Stroke Diagnosis

In case of an ischemic stroke, the existence and the extent of "tissue at risk" surrounding the core of the stroke have to be evaluated. Surgical and medicamentous interventions may salvage at least parts of the "tissue at risk" [7]. In cerebral perfusion, the *first-pass* of the CA (see Fig. 1) is observed. The volume of blood in each voxel is diagnostically relevant. It is approximated by the parameter *Integral*. Other approved parameters are *PE, TTP, MTT* and *Slope* [17].

Case Study. The patient suffered from an infarction in the right hemisphere (which appears left in each view of Fig. 5). The dataset matrix is: 128×128, slice distance: 7 mm, number of slices: 12, temporal resolution: 40 measurements in 40 sec.

Statistical analysis. The results of the statistical analysis are illustrated in Figs. 3-4. First, we added *DownSlope* and *MiTR* to the default parameter set. The correlation coefficients then indicated strong correlations (recall Sec. 4.2): between parameters describing the amount of the enhancement (*Integral* $\leftrightarrow$ *PE*), between parameters describing the velocity of the enhancement (*Slope* $\leftrightarrow$ *MiTR*, *Slope* $\leftrightarrow$ *DownSlope*), and in between these types (*PE* $\leftrightarrow$ *MiTR*, *PE* $\leftrightarrow$ *Slope*). The correlation between *Slope* and *DownSlope* is inversely proportional. Since the *DownSlope* is measured in negative values, this indicates that a fast wash-in (high *Slope* values) is likely to be followed by a fast wash-out (high negative *DownSlope* values). Since *PE* and *Slope* strongly correlate with three other parameters respectively, they have been excluded from further processing.

The PCA showed four major trends (*pc*1-*pc*4) which account for $52\% + 29\% + 11\% + 7\% = 99\%$ of the variance in the data. A problem when interpreting PCA results is to assign a meaning to the newly generated coordinate axes. According to Müller et al. [21], we label the axes with respect to the parameters that determine the trend in the respective pc. More meaningful labels could be "Amount and Velocity" for *pc*1 and "Time to Enhancement" for *pc*2. Interestingly, the trends represented by *pc*3 and *pc*4 characterize atypical enhancement behavior and conflict with *pc*2 and *pc*1, respectively (see Fig. 4). This observation has been further investigated and the results are presented on the website mentioned above.
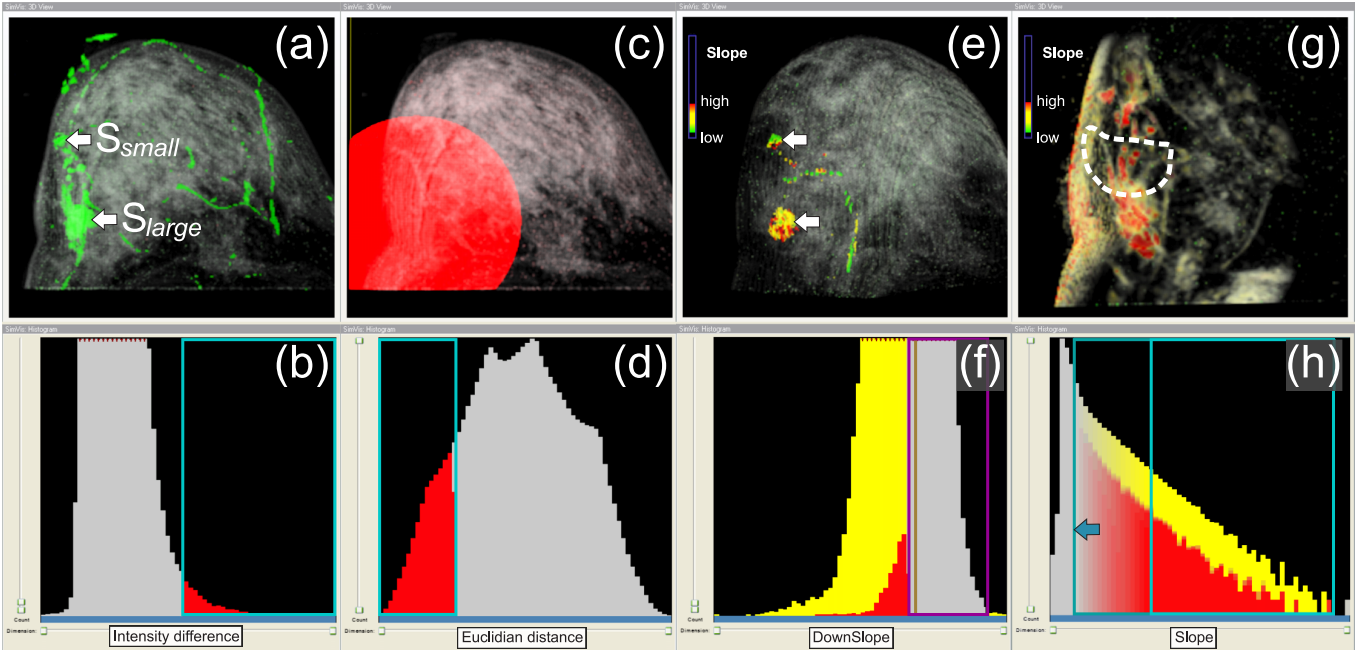
Fig. 6. Breast tumor diagnosis. Selection of high intensity differences between original time points t_2 and t_0 (b) emphasizes areas were the CA is absorbed (a). Two suspicious regions are detected (arrows). The analysis is focused on a local region LR around S_{large} (c) by means of brushing small Euclidian distances between its center and the surrounding tissue (d). Areas exhibiting a rapid wash-out are selected in a histogram depicting *DownSlope* (f). A negative brush (purple box) is used to exclude positive and small negative values. The brown line marks the vertical zero axis. The remaining areas are visualized in (e) and color-coded according to *Slope*. Yellow to red areas indicate a rapid wash-in and wash-out. A smooth brushing of *Slope* within LR (h) reveals subtle jags along the border of S_{large} (g) which are typical for malignant tumors.

Visual analysis. A crucial task in stroke diagnosis is to localize the infarction core and especially the surrounding "tissue at risk". Fig. 5 shows how visual analysis may guide this process. In a scatterplot, TTP and *Integral* are opposed and a region is brushed that indicates delayed and diminished perfusion (Fig. 5 (b)). As a result of this *feature localization*, the infarction core appears as a bright region (Fig. 5 (a)). High TTP values are mapped to colors from yellow to red. Smooth brushing now gives a hint on "tissue at risk" (Fig. 5 (d)). A near-focus region is defined (arrows point at its borders) incorporating areas where the perfusion is delayed as well, however, enough blood arrives over time. Candidate areas for "tissue at risk" appear greenish (medium TTP values) in Fig. 5 (c). This observation could be successfully validated with [16] where the same dataset has been examined. In Fig. 5 (e), the brain has been rotated to illustrate the over-all extension of the infarction. Furthermore, the shape of the brain is indicated as context information. Latter has been achieved by a smooth brushing of the gradient magnitude computed based on the intensity values from a single time point of the original perfusion data (Fig. 5 (f)). This technique will be used throughout the paper. In Fig. 5 (h), the scores of $pc1$ and $pc2$ have been opposed. As discussed above, meaningful axes labels could be "Amount and Velocity" and "Time to Enhancement". Hence, small values on the x-axis and high values on the y-axis are brushed. The near-focus region is selected accordingly. A comparison of Fig. 5 (g) and Fig. 5 (c) shows that the revealed areas match closely. Hence, the trends expressed by $pc1$ and $pc2$ together facilitate the detection of infarcted tissue.

5.2 Breast Tumor Diagnosis

The major diagnostic task in breast tumor diagnosis is to assess the malignancy of a tumor. Evaluating the shape of the TICs has proven to be effective in the differentiation of enhancing lesions [18]. Parameters that describe the shape are *MTT, MiTR, PE, Slope, DownSlope, TTP* and *Integral*. Curves—which show a rapid wash-in followed by a rapid wash-out—are especially suspicious because they indicate strong perfusion and high permeability of vessels. Less suspicious are curves showing a plateau later on, or regions which continue to enhance.

Case Study. The data was acquired to examine a suspicious region in the right mamma which had been detected during conventional mammography. The dataset matrix is: 458×204, slice distance: 3 mm, number of slices: 26, temporal resolution: 6 measurements in 10 min.

Statistical analysis. Two extra parameters describing the steepness of the curve during wash-in and wash-out have been added to the default parameter set. Each of them was computed between two particular time points selected by the user. A strong correlation between *Integral* and *PE* as well as between *PE* and *Slope* was found. Since *PE* strongly correlates with two other parameters, it has been excluded from further processing. The PCA showed four major trends expressed by $pc1$-$pc4$. All together account for $\approx 91\%$ of the variance in the data. In the following, the focus is on a streamlined localization and separation of suspicious structures for *local investigation*.

Visual analysis. Subtraction images emphasize regions where the CA is absorbed (see Sec. 3). Hence, additional parameters have been derived based on the original time points in the perfusion data. Each parameter describes the intensity difference between two subsequent time points t_j and t_i, where $j > i$. In Fig. 6 (b), high differences in intensity between time points t_2 and t_0 have been selected (*Selection*1). The corresponding areas are emphasized in Fig. 6 (a). The structure S_{large} had already been detected in conventional mammography. Furthermore, a smaller structure S_{small} is revealed close to the thoracic wall. Besides these structures, major vessels and the acromastium are emphasized. To focus the analysis on a region around S_{large} for *local investigation*, Euclidean distances between its center and the surrounding tissue are computed. Then, a range of distance values (*Selection*1$_1$) within *Selection*1 is brushed such that the local region LR around S_{large} includes S_{small}. The definition of a local region around S_{large} is illustrated in Fig. 6 (c,d). In Fig. 6 (f), *Selection*1$_1$ (red bars) is transferred to a histogram of parameter *DownSlope* for *multi-variate analysis*. High negative values indicating a rapid wash-out are typical for malignant tumors. Hence, this range has been selected within *Selection*1$_1$ by excluding positive and small negative values with the help of a negative brush (purple box). The result is color-coded by means of parameter *Slope* in Fig. 6 (e). S_{large} and
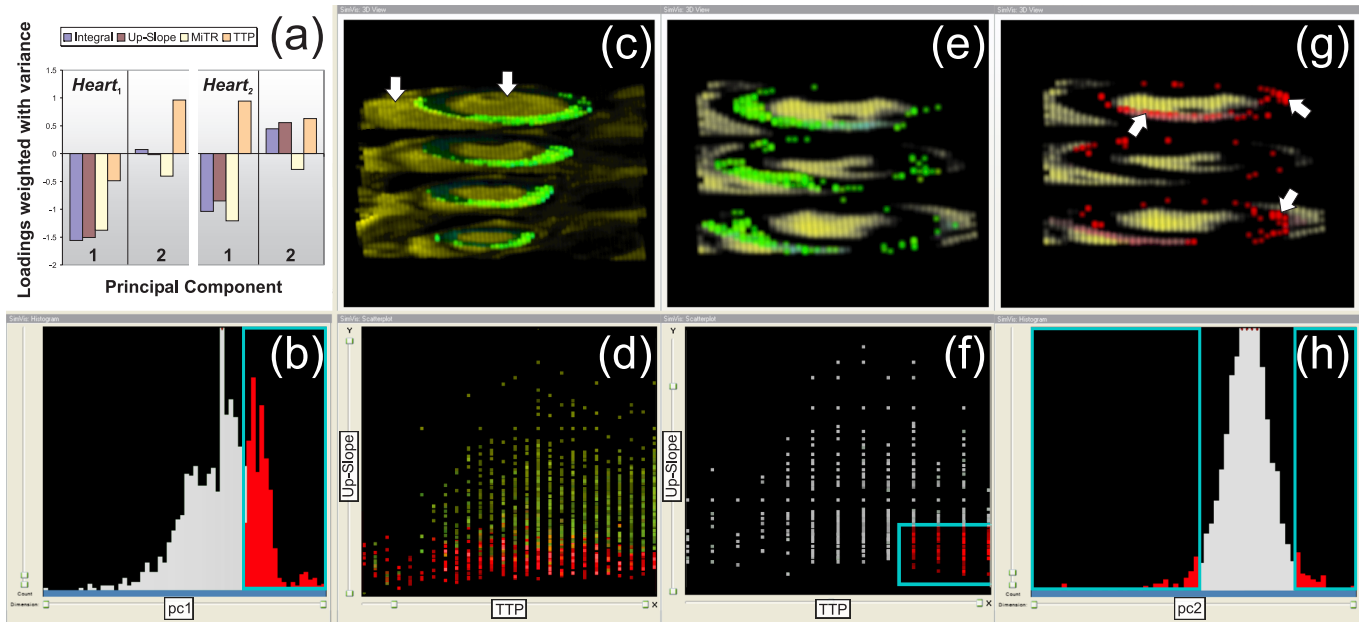
Fig. 7. Visual analysis in CHD diagnosis of datasets $Heart_1$ *(a-d)* and $Heart_2$ *(a, e-h)*. *(a):* Plot representing $pc1$ and $pc2$ of datasets $Heart_1$ and $Heart_2$. Brushing the scores of $pc1$ *(b)* reveals the infarcted region (green area in *(c))*. The right ventricle (left arrow) and the lumen (right arrow) are presented as context information. The selection from *(b)* is transferred to a scatterplot *(d)* opposing TTP and *Up-Slope*. In this case, TTP is not a reliable parameter to detect the infarcted tissue since the selection is spread over its entire codomain (red dots). However, this may not be valid for another dataset as illustrated in *(e-f)* for $Heart_2$. A selection of high TTP values and small *Up-Slope* values *(f)* reveals the infarcted tissue (green area in *(e))*. Brushing the scores of $pc2$ *(h)*, which represents an atypical enhancement pattern, exhibits areas where the motion-correction and thus the segmentation of the myocardium have partially failed *(g)*.

S_{small} both exhibit regions with a rapid wash-in and wash-out and are thus likely to be malignant. S_{small} partially shows small *Slope* values which should be further investigated. Another indication that confirms the suspicion of malignancy is illustrated in Fig. 6 (g-h). A smooth brushing of high and medium *Slope* values within *LR* shows subtle jags (so-called *spikulae*) along the border of S_{large}. The observations in this section could be validated by means of a report from an experienced radiologist who supposed that S_{small} forms a satellite lesion connected to S_{large} by one of the spikulae.

5.3 CHD Diagnosis

In CHD diagnosis, the detection and localization of a perfusion deficit as well as the assessment of the severity are relevant. Major diagnostic tasks to be performed are to evaluate whether the patient suffers from CHD, to evaluate the severity of the disease and to assess the vascular supply of less perfused tissue. At an early stage, CHD is characterized by a perfusion defect caused by a stenosis (an abnormal vessel narrowing). For CHD diagnosis, the parameters *Up-Slope, PE, TTP* and *Integral* have been approved [1], [24], and [25].

Case Study. The two patients both suffered from a heart attack. The matrix of dataset $Heart_1$ is: 144×192, slice distance: 18 mm, number of slices: 4, temporal resolution: 40 measurements in 38 sec. The matrix of dataset $Heart_2$ is: 144×192, slice distance: 18 mm, number of slices: 3, temporal resolution: 40 measurements in 23 sec.

Statistical analysis. First, *MiTR* has been added to the default parameter set. The correlation coefficients for $Heart_1$ and $Heart_2$ indicated a strong correlation between *Integral* and *PE*. Due to the higher variance of the *Integral* values in both cases, *PE* was excluded from the PCA. The PCA of $Heart_1$ showed two major trends in $pc1$ and $pc2$, respectively (Fig. 7 (a)). Both pc's together explain $\approx 91\%$ of the variance in the data. However, $pc1$ describes an atypical enhancement pattern. In damaged tissue, the blood flow is delayed (high TTP values) and diminished (low *Integral* values). However, $pc1$ indicates a proportional relationship which will be examined below.

The PCA of $Heart_2$ showed three major trends expressed by $pc1$ to $pc3$. All together account for $51\% + 25\% + 17\% = 93\%$ of the vari-

ance in the data. For the sake of brevity, only the first two pc's are examined here (Fig. 7 (a)). A typical enhancement pattern is represented by $pc1$. However, $pc2$ shows an atypical pattern. As in $pc1$ of $Heart_1$, TTP is proportional to *Integral* and *Up-Slope*. Furthermore, *MiTR* is inversely proportional to *Up-Slope* though both parameters describe the steepness of the curve during wash-in.

Visual analysis. To examine the atypical enhancement pattern represented by $pc1$ of $Heart_1$, the scores of $pc1$ have been brushed in a histogram (Fig. 7 (b)). A selection of high values reveals the infarcted tissue (green region in Fig. 7 (c)) within the ring-shaped myocardium. Since the circular shape of the myocardium hampers the orientation, context information has been added. Two arrows point at the right ventricle (left arrow) and the lumen of the left ventricle (right arrow). The selection from Fig. 7 (b) has been transferred for a *multi-variate analysis* to a scatterplot opposing TTP and *Up-Slope* (red dots in Fig. 7 (d)). Interestingly, the infarcted tissue is spread over all time points. Probing the TICs within the infarcted region showed that the acquisition time of the scan was too short to determine a reliable TTP. In the infarcted region, no CA arrived at all over time. However, *PE* and therefore TTP always exist—no matter if the TIC represents CA enhancement or noise. After all, it seems that in spite of the unreliable TTP values a brushing of the scores of $pc1$ still delivers meaningful results. This might be due to the low loading of TTP (Fig. 7 (a)).

A major difficulty in analyzing perfusion data is that the reliability of a parameter may change from case to case. As illustrated in Fig. 7 (a, e, f), TTP might be a reliable parameter for *feature localization* in $Heart_2$. Brushing of high TTP and small *Up-Slope* values reveals the infarcted region (green). Here, $pc1$ describes a typical enhancement pattern. In contrast, $pc2$ describes an atypical pattern: TTP and *Integral* are proportional, and *Up-Slope* and *MiTR* are inversely proportional related. Brushing of extreme values of $pc2$ (Fig. 7 (h)) reveals areas at the transitions between myocardium and lumen and myocardium and pericardium (Fig. 7 (g)). Further examination showed that the propagation of the segmented myocardial contours did not match the myocardium at all time points (recall para. Pre-processing in Sec. 5). It turned out that the motion correction had partially failed.

6 SUMMARY AND CONCLUSION

We presented the integration of pre-processing techniques, statistical methods, and interactive feature specification for the analysis of the multi-dimensional space of perfusion parameters. The visual analysis strategy presented here allows to assess the reliability of specific perfusion parameters, the correlation of perfusion parameters in a particular case, and thus enables an efficient evaluation focused on a significant subset of perfusion parameters. The statistical analysis facilitates the detection of trends in the data. Trends, representing typical enhancement patterns, may be applied for the detection of suspicious structures while trends, representing atypical enhancement patterns, may indicate pre-processing failures. We discussed our approach with two experienced radiologists, both familiar with perfusion imaging in the clinical routine, though not in a research context. Both argued that the statistical analysis is only applicable in the clinical routine—in particular in emergency cases—if carried out in the background leading to an initial suggestion for suspicious regions. We will investigate this in our future work. Both assessed brushing as valuable for exploring a non-standardized parameter domain. They appreciated the visualization of perfusion data in 3D since it provides a good overview.

Compared to the prevailing visual and highly subjective evaluation methods, our approach enables a more reproducible evaluation supported by quantitative analysis results. Thus, it may be used to answer questions regarding the diagnostic value of certain parameter combinations and to investigate the effects of a new contrast agent or changes in other imaging parameters on this value. Such questions are debated in the medical research. The most important work to be done relates to a thorough evaluation for a larger number of specific cases in cerebral, tumor, and myocardial perfusion. Within such an evaluation, the perfusion data analysis and clinical parameters characterizing the progress of the respective disease have to be integrated to better understand the diagnostic value of perfusion parameters.

SimVis has been designed to work with data laid out on arbitrary grids. An overhead of neighborhood information is generated for medical data laid out on Cartesian grids. This overhead hampered an interactive analysis in case of DCE-MRIM data exhibiting a high spatial resolution. Techniques from [3] will be investigated to resolve this limitation. With respect to the analysis strategy, the incorporation of clustering techniques which classify regions according to the similarity of TICs, deserves a systematic investigation.

ACKNOWLEDGEMENTS

REFERENCES

[1] N. Al-Saadi, M. Gross, A. Bornstedt, B. Schnackenburg, C. Klein, E. Fleck, and E. Nagel. Comparison of various parameters for determining an index of myocardial perfusion reserve in detecting coronary stenosis with cardiovascular magnetic resonance tomography. *Z Kardiol*, 90(11):824–34, Nov 2001.

[2] U. Behrens, J. Teubner, C. J. Evertsz, M. Walz, H. Jürgens, and H.-O. Peitgen. Computer-Assisted Dynamic Evaluation of Contrast-Enhanced-MRI. In *Proc. of Computer Assisted Radiology*, pages 362–367, 1996.

[3] J. Blaas, C. Botha, and F. Post. Interactive visualization of multi-field data using dynamically linked physical and feature space views. In *Proc. of EuroVis*, pages 123–130, 2007.

[4] W. Chen, M. Giger, U. Bick, and G. Newstead. Automatic identification and classification of characteristic kinetic curves of breast lesions on DCE-MRI. *Medical Physics*, 33(8):2878–2887, 2006.

[5] P. L. Choyke, A. J. Dwyer, and M. V. Knopp. Functional tumor imaging with dynamic contrast-enhanced magnetic resonance imaging. *J Magn Reson Imaging*, 17(5):509–20, May 2003.

[6] E. Coto, S. Grimm, S. Bruckner, E. Gröller, A. Kanitsar, and O. Rodriguez. MammoExplorer: An Advanced CAD Application for Breast DCE-MRI. In *Proc. of VMV*, pages 91–98, 2005.

[7] J. A. den Boer and P. J. M. Folkers. MR perfusion and diffusion imaging in ischaemic brain disease. *Medica Mundi*, 41(2):20–35, 1997.

[8] H. Doleisch, M. Gasser, and H. Hauser. Interactive Feature Specification for Focus+Context Visualization of Complex Simulation Data. In *Proc. of IEEE TCVG - EUROGRAPHICS Symp. on Vis.*, pages 239–248, 2003.

[9] H. Doleisch and H. Hauser. Smooth brushing for focus+context visualization of simulation data in 3D. *Journal of WSCG*, 10(1):147–154, 2002.

[10] G. Furnas. Generalized fisheye views. In *Proc. of the ACM CHI '86 Conf. on Human Factors in Computing Systems*, pages 16–23, 1986.

[11] D. L. Gresh, B. E. Rogowitz, R. L. Winslow, D. F. Scollan, and C. K. Yung. WEAVE: A System for Visually Linking 3-D and Statistical Visualizations, Applied to Cardiac Simulation and Measurement Data. In *Proc. of IEEE Visualization*, pages 489–492, 2000.

[12] H. K. Hahn and H.-O. Peitgen. The skull stripping problem in MRI solved by a single 3d watershed transform. In *Proc. of MICCAI*, volume 1935 of *LNCS*, pages 134–143. Springer, 2000.

[13] H. Hauser. Generalizing focus+context visualization. In *Scientific Visualization: The Visual Extraction of Knowledge from Data*, pages 305–327, 2005.

[14] G. Hellwig, G. Brix, J. Griebel, R. Lucht, S. Delorme, M. Siebert, and K.-H. Englmeier. Dynamic MR mammography: three-dimensional real-time visualization of contrast enhancement in virtual reality. *Academic Radiology*, 9:1255–1263, 2002.

[15] I. T. Jolliffe. *Principal Component Analysis*. Series in Statistics. Springer, 2nd edition, 2002.

[16] S. Kohle, B. Preim, J. Wiener, and H.-O. Peitgen. Exploration of Time-varying Data for Medical Diagnosis. In *Proc. of VMV*, pages 31–38, 2002.

[17] M. König, E. Klotz, and L. Heuser. Perfusion CT in Acute Stroke: Characterization of Cerebral Ischemia using Parameter Images of Cerebral Blood Flow and their Therapeutic Relevance. *Electromedica*, 66(2):61–67, 1998.

[18] C. K. Kuhl, P. Mielcareck, S. Klaschik, C. Leutner, E. Wardelmann, J. Gieseke, and H. H. Schild. Dynamic Breast MR Imaging: Are Signal Intensity Time Course Data Useful for Differential Diagnosis of Enhancing Lesions? *Radiology*, 211(1):101–110, 1999.

[19] M. Lysaker, A. Lundervold, and X. Tai. Noise Removal Using Fourth-Order Partial Differential Equation with Applications to Medical Magnetic Resonance Images in Space and Time. *IEEE Trans. Image Processing*, 12(12):1579–1590, 2003.

[20] M. Mlejnek, P. Ermes, A. Vilanova, R. van der Rijt, H. van den Bosch, E. Gröller, and F. Gerritsen. Application-oriented extensions of profile flags. In *Proc. of EuroVis*, pages 339–346, 2006.

[21] W. Müller, T. Nocke, and H. Schumann. Enhancing the visualization process with principal component analysis to support the exploration of trends. In *Proc. of Asia-Pacific Symposium on Information Visualisation*, pages 121–130, 2006.

[22] T. Nattkemper and A. Wismuller. Tumor feature visualization with unsupervised learning. *Medical Image Analysis*, 9(4):344–351, 2005.

[23] S. Oeltze, F. Grothues, A. Hennemuth, A. Kuß, and B. Preim. Integrated Visualization of Morphologic and Perfusion Data for the Analysis of Coronary Artery Disease. In *Proc. of EuroVis*, pages 131–138, 2006.

[24] I. Paetsch, C. Jahnke, A. Wahl, R. Gebker, M. Neuss, E. Fleck, and E. Nagel. Comparison of Dobutamine Stress Magnetic Resonance, Adenosine Stress Magnetic Resonance, and Adenosine Stress Magnetic Resonance Perfusion. *Circulation*, 110(7):835–842, 2004.

[25] J. R. Panting, P. D. Gatehouse, G. Z. Yang, M. Jerosch-Herold, N. Wilke, D. N. Firmin, and D. J. Pennell. Echo-planar magnetic resonance myocardial perfusion imaging: parametric map analysis and comparison with thallium SPECT. *J Magn Reson Imaging*, 13(2):192–200, Feb 2001.

[26] D. Rueckert, L. Sonoda, C. Hayes, D. Hill, M. Leach, and D. J. Hawkes. Nonrigid registration using free-form deformations: application to breast MR images. *IEEE Trans. Med. Imag.*, 18(8):712–721, 1999.

[27] A. Schenk, G. Prause, and H.-O. Peitgen. Efficient semiautomatic segmentation of 3d objects in medical images. In *Proc. of MICCAI*, pages 186–195. Springer, 2000.

[28] T. Twellmann, O. Lichte, and T. Nattkemper. An adaptive tissue characterization network for model-free visualization of dynamic contrast-enhanced magnetic resonance image data. *IEEE Trans. Med. Imag.*, 24(10):1256–1266, 2005.